IEEE Access
Multidisciplinary | Rapid Review | Open Access Journal

Received August 20, 2019, accepted September 3, 2019, date of publication October 16, 2019,
date of current version November 30, 2021.

Digital Object Identifier 10.1109/ACCESS.2019.2945919

A Comprehensive VSG-Based Onshore FRT Control Strategy for OWFs With VSC-MT-HVDC Transmission

SEYED SAEID HEIDARY YAZDI[1], JAFAR MILIMONFARED[1], SEYED HAMID FATHI[1], AND KUMARS ROUZBEHI[2], (Senior Member, IEEE)

[1]Department of Electrical Engineering, Amirkabir University of Technology, Tehran 15875-4413, Iran
[2]Department of Electrical Engineering, University of Seville, 41004 Seville, Spain

Corresponding author: Seyed Saeid Heidary Yazdi (saedheidary@aut.ac.ir)

ABSTRACT This paper proposes a communication-free control strategy at the offshore wind farm (OWF) level to enhance onshore fault ride-through (FRT) grid code compliance of the voltage source converter (VSC)-based multi-terminal high voltage direct current (MT-HVDC) grid. In this proposal, the emerging virtual synchronous generator (VSG) concept is employed to equip the Type 4 wind turbine generator (WTG)s with inherent grid forming ability. Accordingly, it is proposed to switch the offshore HVDC converters control mode from grid forming to grid feeding during onshore FRT period to realize direct wind power in-feed reduction as a function of the severity of MT-HVDC grid's overvoltage. The related dynamics are mainly characterized by the high-speed current control loop, so improved OWF response is achieved during onshore FRT period as conventional voltage/frequency modulation strategies are not employed. New analysis/amendments are also proposed to study and improve the transient active power reduction sharing between the WTGs in first few power cycles under wind wake effect. Finally, with the objective of a smooth transfer of HVDC converters and WTGs in several proposed operation states, a set of state machines are proposed considering whole WTG's dynamics. Comprehensive time-domain simulations are performed with averaged electromagnetic transient models to demonstrate the improved onshore FRT behavior in terms of minimizing the electrical stress at both MT-HVDC grid and OWF levels.

INDEX TERMS Fault-ride-through, multi-terminal HVDC grid, offshore wind farm, power reduction method, type 4 WTG, virtual synchronous generator.

NOMENCLATURE

ACC	AC Collection
APL	Active Power Limiter
DSOGI	Dual Second Order Generalized Integrator
EMF	Electro-Magnetic Force
EMT	Electro-Magnetic Transient
EPRP	Energy Per Rated Power
FD-PSACR	Frequency-Dependent-Positive Sequence Active Current Reduction
FRT	Fault Ride Through
GC	Grid Code
GSC	Grid Side Converter
HVDC	High Voltage Direct Current
MPPT	Maximum Power Point Tracking
MSC	Machine Side Converter
MT	Multi-Terminal
NF	Notch Filter
OF-HVDCC	OFfshore HVDC Converter
ON-HVDCC	ONshore HVDC Converter
OWF	Offshore Wind Farm
PF	Power Flow
PI	Proportional Integral
PLC	Power Loop Control
PLL	Phase-Locked Loop
PMSG	Permanent Magnet Synchronous Generator
PR	Proportional Resonance
RFO	Rotor Flux Oriented
RoCoF	Rate of Change of Frequency
RPLC	Reactive Power Loop Control
SRF	Synchronous Reference Frame
VCO	Voltage Controlled Oscillator

The associate editor coordinating the review of this manuscript and approving it for publication was Mingjian Cui.

VD-PSACR	Voltage-Dependent Positive Sequence Active Current Reduction
VSC	Voltage Source Converter
VSG	Virtual Synchronous Generator
WTG	Wind Turbine Generator

I. INTRODUCTION

A. PROBLEM STATEMENT

VSC-based MT-HVDC grids integrating the OWFs must meet FRT GC requirements mainly by onshore grid voltage support through extra reactive current injection [1]. However, FRT compliance is challenging due to DC decoupling between onshore and offshore networks. Moreover, significant power imbalance occurs between the reduced active power exported by ON-HVDCCs and the wind power in-feed by OF-HVDCCs which will be stored as an electrical field in the respective capacitors of VSCs and HVDC lines. Accordingly, transient direct over-voltage might appear due to the limited stored EPRP of VSCs that might cause equipment failure/aging in turn [2].

B. LITERATURE REVIEW

There are several strategies to confine the direct overvoltages below the 0.2 pu. The first solution is to provide both shunt and series onshore network connection paths for ON-HVDCC and hence ensure entire wind power delivery or to install dissipative/storage external circuitries [1], [3]–[5]. These solutions are costly but effective, as they usually do not impact the OWF's operating status. The second economic and elaborate solution provides control frameworks at the OWF level to reduce the wind power in-feed effectively [6]– [11]. This can be done by sending active power reduction orders to individual WTGs through a dedicated fast communication channel [10], [12], [13] with reliability concerns. Nevertheless, a suitable supplementary control loop should be implemented in this regard to modulate the WTGs active power reference as a function of the communicated signal. Wind power in-feed reduction can also be done by emulating the fault conditions inside the OWF via the appropriate exercise of OF-HVDCC (e.g., frequency or voltage modulation) with careful tuning [14] that relies on local measurements and controllers. Fast frequency increase is applied in the frequency modulation approach to trigger WTGs dynamic frequency response. However, slow dynamics are envisioned as for frequency measurement delay and limited admissible RoCoF [14]–[17]. In this scheme, a supplementary control loop as a function of OWF's frequency and its derivative is added to the WTGs control software. It is to modulate the WTGs active power reference as a function of OWF's frequency by providing inertial and primary frequency response. On the other hand, undesired controlled voltage reduction is performed in the voltage modulation strategy to exploit the FRT capability of the modern WTGs [6], [7], [12], [14], [16], [18]–[20]. In more details, during voltage dips, WTGs should assign the converters current capacity allocation priority to the reactive current for grid voltage support and grid code following. Accordingly, there will be reduced room for active current delivery; therefore, WTGs active power will be reduced inevitably. However, the challenge of high amplitude short-circuit currents, with possibly a DC component, exists in Type-3 based OWFs with the amendments proposed in [6], [16] that might hinder the effective fast power curtailment.

The described control strategies are done indirectly as the OF-HVDCC requests the individual WTGs to reduce their injected wind power rather than reducing the active power directly by itself, Fig. 1. It is since the voltage of the OWF's ACC network is formed by the OF-HVDCC in voltage/frequency control mode and the WTGs GSC are operated as grid feeding converters in active/reactive power control mode, i.e., conventional PLL units are utilized to achieve grid synchronism that has no grid forming capability. Accordingly, upon switching the OF-HVDCC's control mode to a grid feeding converter in active/reactive power control mode to execute direct wind power in-feed reduction, the OWF ACC network might be unstable due to the absence of a grid former unit.

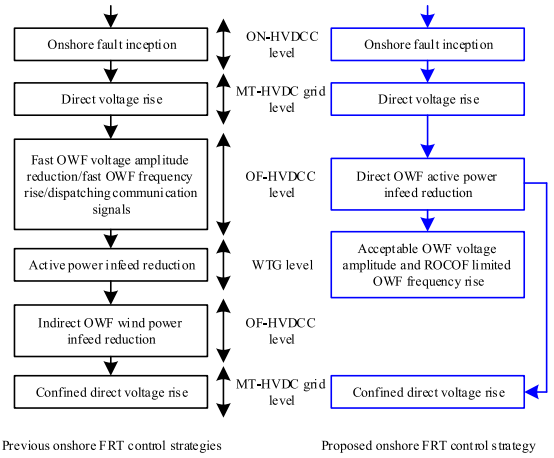

FIGURE 1. Flowchart of the proposed direct wind power in-feed curtailment versus pervious OWF voltage and frequency modulation and communication based onshore FRT control strategies.

C. RESEARCH OBJECTIVE AND CONTRIBUTIONS

This paper proposes a novel, fast, communication-less, and OWF friendly coordinated control framework at the OWF level to reduce the wind power-infeed directly, Fig. 1. In this sense, it is proposed to control the WTGs GSC as VSGs with inherent grid forming ability as the first contribution. Accordingly, the OF-HVDCC's operation mode can be changed from grid forming to grid feeding during direct overvoltage transient period to execute direct and hence very fast wind power in-feed reduction. Effective grid forming ability of the VSGs ensures acceptable voltage magnitude as well as RoCoF limited frequency rise in the ACC networks voltages during the transient period.

The burden of wind power-infeed reduction will be shared between the individual WTGs in the limited few power cycles

TABLE 1. Comparison of different FRT control schemes.

	Communication-based approach	Voltage modulation-based	Frequency modulation-based approach	Proposed VSG-based approach
Advantages	minimum WTG/OF-HVDCC control interaction minimum WTG control modification requirements	fast dynamics communication-free nature low WTG control modification requirements	communication-free nature low WTG control modification requirements	very fast dynamics communication-free nature no fault condition emulation in the OWF limited OWF RoCoF low WTG/OF-HVDCC control interactions
Disadvantages	low reliability slow dynamics	fault condition emulation in the OWF high WTG/OF-HVDCC control interactions hard control tuning possible malfunction of the OWF protection system	high RoCoF emulation in the OWF high WTG/OF-HVDCC control interactions slow dynamics hard control tuning possible malfunction of the OWF protection system	high WTG/OF-HVDCC control modification requirements

of fault period. In this period, the load sharing characteristics are dominated by the pre-fault operating point under the wind wake effect and adopted virtual admittances. In this sense, poor transient load sharing is found according to the developed equations/model. Two proposals, including a suitable virtual admittance tuning method and an APL, are also introduced to improve load sharing characteristics as the *second contribution*.

The proposed control framework implies several operation states starting from fault inception up to the end of the post-fault course considering the proposed control modules for the OF-HVDCC and individual WTGs. In this regard, a set of state machines comprised of suitable switching logics are proposed as the third contribution to coordinate the process of state switching in a seamless fashion and reduce the transient period. Complete WTG dynamics are considered which were neglected in previous studies. Proposed FRT control strategy is compared to previous FRT control strategies in Table I.

II. POWER SYSTEM UNDER STUDY

A generic three-terminal and symmetric monopolar (±200 kV) MT-HVDC grid comprised of time-averaged EMT models, Fig. 2, is considered as the test grid that has the most severe envisioned onshore FRT condition. Onshore network (A0 in Fig. 2) is modeled using an ideal AC source behind the Thévenin impedance. The HVDCCs are designed according to German GC requirements and the related EPRPs are considered to be 45 kJ/MVA [10]. The HVDC cables are modeled by lumped pi models with the parameters of [21] and the associated lengths of Fig. 2. To obtain realistic results

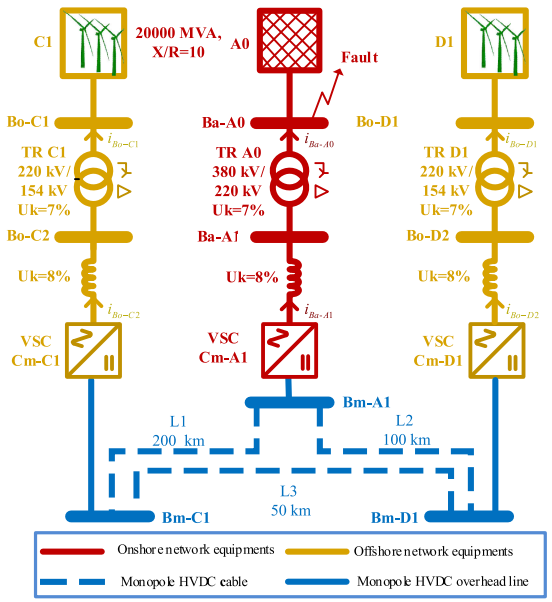

FIGURE 2. Schematic diagram of a generic three-terminal MT-HVDC grid interconnecting OWFs and onshore ac network.

and study the impacts of wind wake effects on the proposed FRT control strategy, detailed model of a (15 × 5 MW) OWF is simulated, Fig. 3 [22]. The associated ACC network is comprised of lumped pi-modeled MV and HV cables as well as step-up transformers divided into three strings ($N_2 = 3$) with 5 Type 4 WTGs ($N_1 = 5$) per string. Entire OWF parameters/models and cable lengths, except the WTGs and OF-HVDCC, are referred to [22].

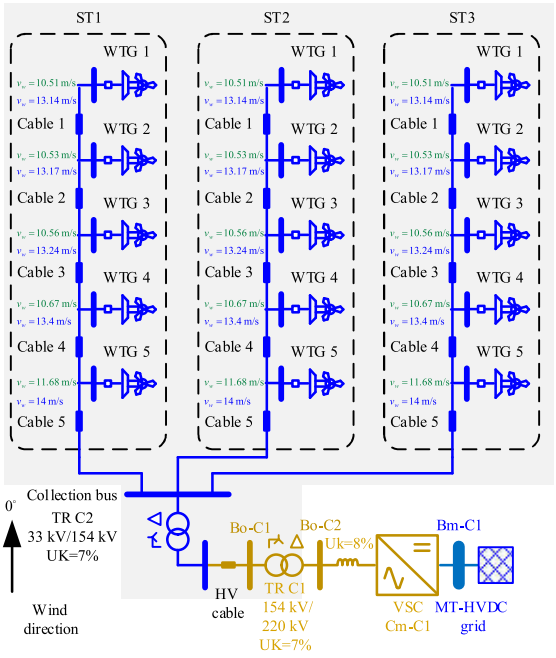

FIGURE 3. Schematic diagram of the test 75 MW OWF connected to central VSC-based OF-HVDCC.

III. MODELING AND CONTROL OF ON-HVDCC AND OF-HVDCCS

A. ON-HVDCC

The ON-HVDCC aims to transfer the captured OWFs wind energy to the onshore AC network and satisfy grid code requirements [23]–[25]. The employed cascaded control scheme and its governing state machine are depicted in Fig. 4 and Fig. 5 respectively. It includes a dual SRF current vector control scheme, that is synchronized to positive sequence ac network voltage (u_{abc+}) using DSOGI filters, to generate ON-HVDCC's switching functions (s_j, $j = a, b, c$) [5]. Zero sequence components will be absent as for the Y_g/Δ connection of the ON-HVDCC transformer.

1) BASIC CONTROL TASKS IN THE POSITIVE SEQUENCE

The ON-HVDCC is operated under the S1 operation state of Fig. 5 initially. The basic converter control tasks in this state include pole-to-pole direct voltage (v_{dc}) and AC voltage amplitude regulation using i^*_{d+} and i^*_{q+} specification with current (i) priority given to the i^*_{d+}. In the whole paper, the $+$, $-$, 0, d, and q subscripts denote positive sequence, negative sequence, last measured, direct axis, and quadrant axis value of the related variable. Also, the superscript ($*$) refers to the reference of the related variable.

The operation state will be switched to the S2 with the current priority given to the i^*_{q+} once the positive sequence terminal voltage (u_{d+}) is lower than u^{ther2}_{d+} threshold ($u_{d+} < u^{ther2}_{d+}$) but $i^*_{d+} > 0$ condition still holds.

Upon state switching, the AC voltage regulator will be frozen to avoid integrators excursion ($EN_1 = 0$). The i^*_{q+} is specified by the $i^*_{q+} = i^*_{q0+} + k_{iq+u}(u_{d+} - u^{ther2}_{d+})$ relation under balanced onshore FRT conditions ($\min(i^*_{q+}) = -1.08\ pu$ and $k_{iq+u} = 2$) for GC-based network voltage support. Hence, a considerable reduction of i^*_{d+} is expected that is undesirable. Also, the output of the PI-based direct voltage controller, which embeds suitable anti-wind-up protection, will be dynamically limited to maximum allowable i^*_{d+} specified by the VSC current modulus limiter. Once $u_{d+} > u^{ther2}_{d+}$, the operation state will be returned to S1.

Nevertheless, if $i^*_{d+} \approx 0$ while operating in the S2, the operation state will be switched to the S3 that embeds identical control modules. It is except the post-FRT maneuvers that the operation state will be switched to ramp up state (S4) rather than direct return to S1. The ramp up state projects to come up with a smooth pre-defined i_{d+} recovery slope ($R_{postFRTslope}$) in pu/s that has a certain impact on the transient stability of the onshore power system and magnitude and duration of the post-fault direct overvoltage [26].

Finally, the operation state will be returned to the S1 once the v_{dc} reaches the vicinity of the related pre-fault reference. The steady-state i^*_{d+} will be determined by the total wind energy captured by OWFs that is likely to be unchanged compared to pre-FRT condition for high $R_{postFRTslope}$ slopes that imply a short transient period.

2) BASIC CONTROL TASKS IN THE NEGATIVE SEQUENCE

In this research, the i^*_{dq-} are determined as (1) to remove the DSF oscillations within the 3ϕ transmitted active power and hence the stress on the direct voltage (as well as related protection units) will be minimized during unbalanced FRT conditions.

$$\begin{bmatrix} i^*_{d-} \\ i^*_{q-} \end{bmatrix} = -\begin{bmatrix} u_{d+} & u_{q+} \\ -u_{q+} & u_{d+} \end{bmatrix}^{-1} \begin{bmatrix} u_{d-} & u_{q-} \\ u_{q-} & -u_{d-} \end{bmatrix} \begin{bmatrix} i^*_{d+} \\ i^*_{q+} \end{bmatrix} \quad (1)$$

3) EMPLOYED VSC CURRENT MODULUS LIMITATION SCHEME

A VSC current modulus limitation scheme is adopted to employ full safe current capacity of the VSCs under both normal and transient conditions. It is to reach maximum FRT active power delivery [5] while considering the adopted philosophy for i^*_{dq-} determination, employed dual SRF vector control strategy, and sinus-based Park transformations. The core idea is a predefined step-wise reduction of the initial i^*_{dq+} components according to their priority until preserving semiconductor safety. The VSC tracks last specified pre-fault i^*_{dq+-} values before calculation of new i^*_{dq+-} values to ensure successful operation.

B. OF-HVDCC

The OF-HVDCC is responsible for injecting the OWF energy to the HVDC link by behaving as a slack AC voltage source with constant voltage amplitude, phase angle, and frequency for the ACC network. This grid forming act is done by employing the control scheme shown in Fig. 6 in which the frequency reference unit provides frequency and angle information required for Park/Clark transformations.

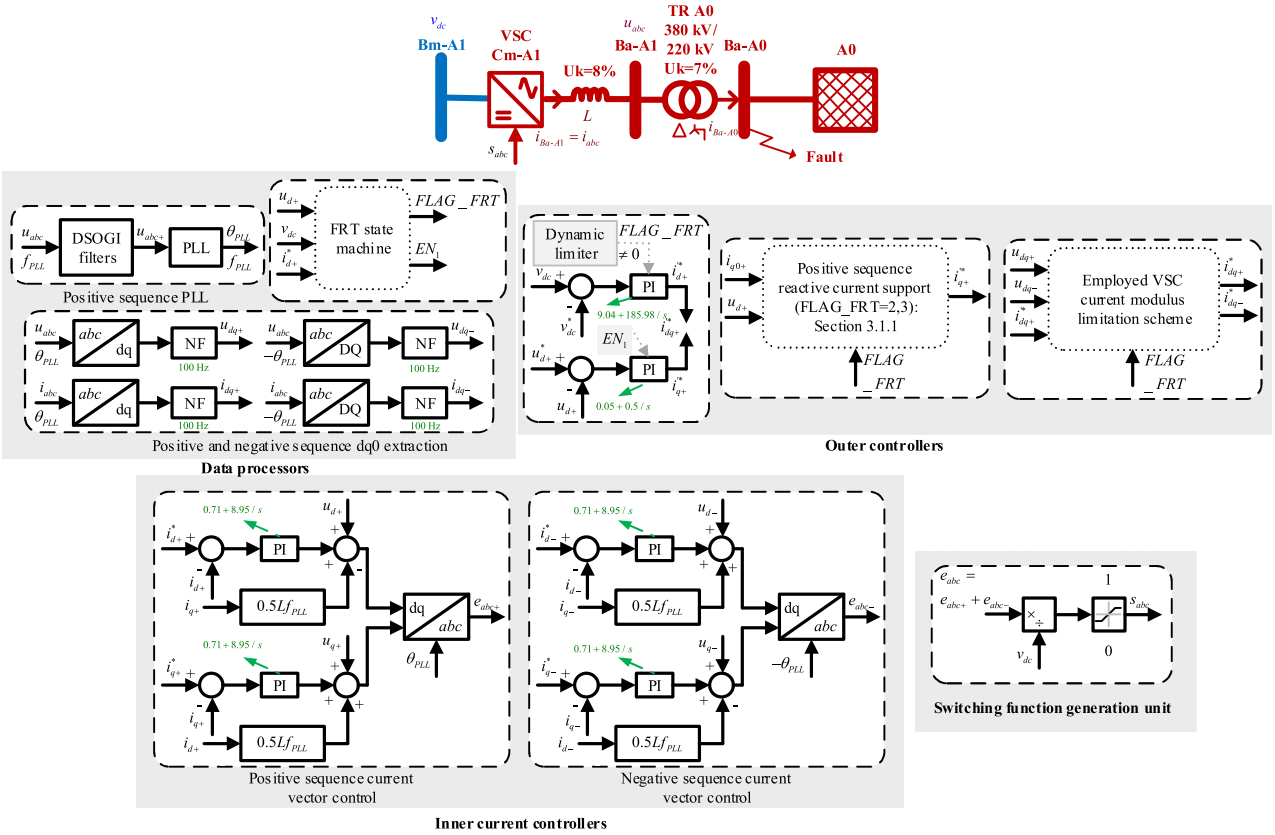

FIGURE 4. Implemented cascaded control structure at the ON-HVDCC comprised of the data processor, positive sequence PLL, dual SRF control scheme, employed VSCs current modulus limiter, and outer current reference calculator units.

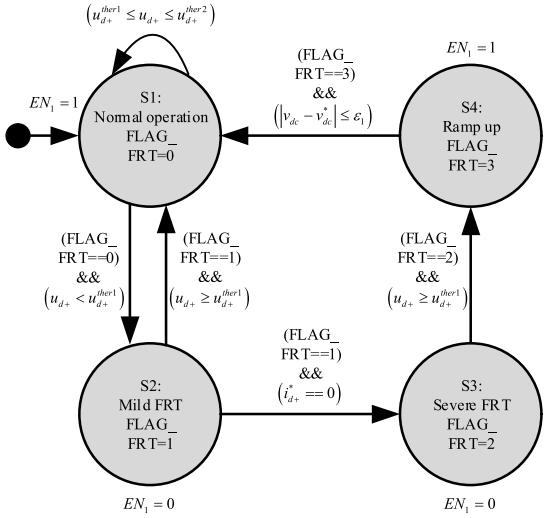

FIGURE 5. Employed state machine to coordinate the operation of the ON-HVDCC between normal, mild FRT, severe FRT, and ramp up states during FRT period ($u_{d+}^{ther1} = 0.9$ *pu*, $u_{d+}^{ther2} = 1.1$ *pu*, $\varepsilon_1 = 0.005$ *pu*) [14], [20].

Accordingly, suitable VSC inner EMF voltage e_{abc} is generated by processing the regulation error of OF-HVDCC's terminal voltage (u_{dq}). The enabling status of the control modules in each operation state is clear from the proposed state machine of Fig. 8 which is designed to avoid integrator states excursion of controllers.

1) PROPOSED FRT CONTROL STRATEGY AND THE GOVERNING STATE MACHINE

The proposed control strategy for direct wind power-infeed reduction can be described by the control scheme of Fig. 6 and the related proposed governing state machine of Fig. 8. Once the direct voltage at the VSCs bus (v_{dc} in Fig. 6) exceeds the predefined threshold of v_{dc}^{ther}, the operation state will be switched to wind power-infeed reduction (S2) state. In this state, the OF-HVDCC is operated as a grid feeding converter, i.e., a backup PLL provides the required frequency and angle information required for Park/Clark transformations rather than the frequency reference unit. Besides, the d-axis (active) converter current reference (i_d^*) is reduced from the last value recorded in S1 state (i_{d0}) as a function of measured direct voltage (v_{dc}) and is tracked by an activated inner vector current control unit:

$$i_d^* = i_{d0} - k_{pc}(v_{dc} - v_{dc}^{ther}) \tag{2}$$

The k_{pc} is designed to null the whole transmitted active current at the technical limit of $v_{dc}^{\max} = 1.2$ p.u., hence $k_{pc} = 1/(v_{dc}^{\max} - v_{dc}^{ther})$. However, extra reliability can be envisioned by selecting a relatively lower $v_{dc}^{\max}$ of 1.18 pu. Thanks to

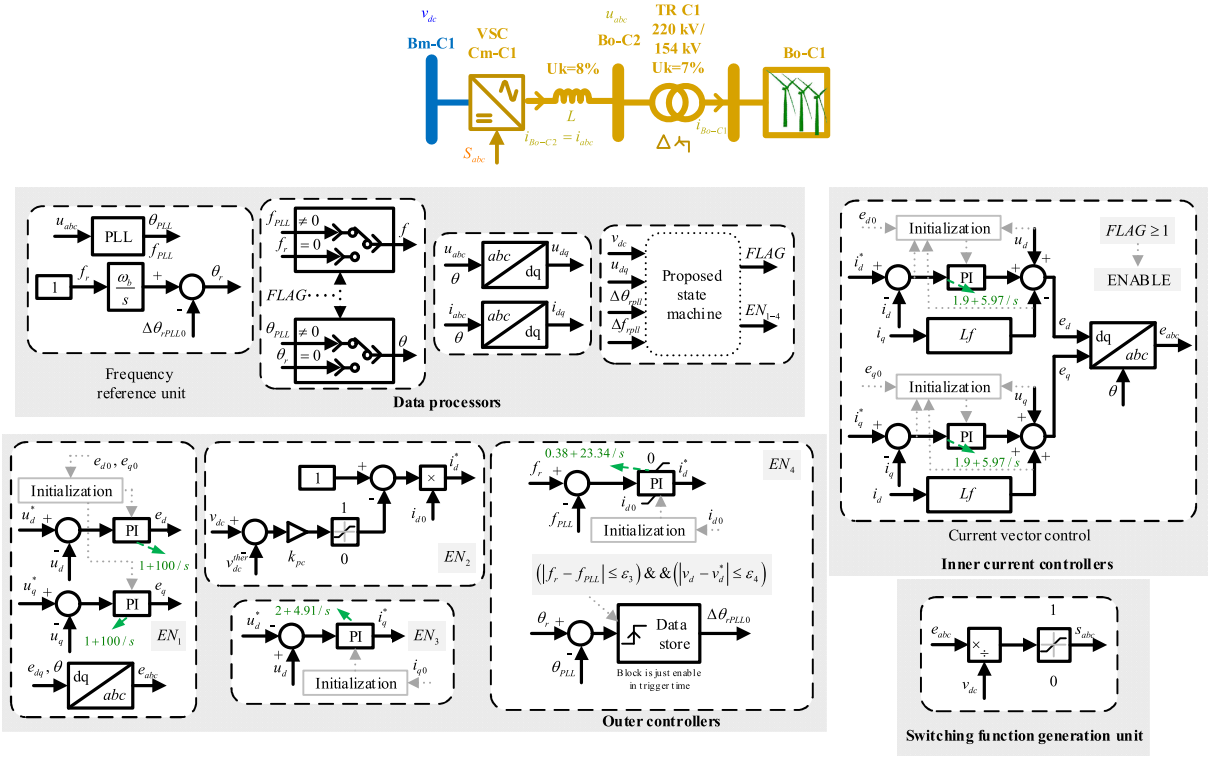

FIGURE 6. Implemented control structure at the OF-HVDCC and proposed control strategy for direct wind power-infeed reduction ($\omega_b = 2\pi \times 50$ rad/s, $u_d^* = 1$ pu.$u_q^* = 0$ pu, $\Delta\theta_{rpll} = \theta_r - \theta_{PLL}$, $\Delta f_{rpll} = f_r - f_{PLL}$, $v_{dc}^{ther} = 1.05$ pu, $\Delta f^{max} = 0.25/50$ pu, $\Delta f_r^{max} = 0.1/50$ pu).

the high bandwidth of the current control loop, a rapid wind power-infeed reduction and hence confined direct voltage rise are expected. Meanwhile, an AC voltage controller is activated to regulate the d-axis ACC network's voltage at OF-HVDCC terminal to unity by specifying suitable q-axis converter current reference (i_q^*) as (3). However, the related q-axis voltage component will be effectively zero due to the action of the enabled PLL.

$$i_q^* = i_{q0} + \left(k_{pvd} + \frac{k_{ivd}}{s}\right) \cdot \left(u_d - u_d^*\right) \tag{3}$$

The ACC network's voltages will be effectively formed by the VSG-controlled WTGs in S2 and S3 states. Accordingly, voltage amplitude of ACC network's buses will effectively remain within an acceptable range and the related frequency rise will have a limited RoCoF due to the emulated inertia. The operation state will be switched to the OWF recovery state (S3) if these conditions are met:

- The direct voltage falls below the v_{dc}^{ther} , i.e. the onshore fault is cleared.
- The actual three-phase voltage at the OF-HVDCC terminal is not sufficiently overlapped with the related reference specified by the frequency reference unit of Fig. 6 which will be activated again in the S1 operation state.

The overlap condition states that the frequency, phase angle, sequence, and amplitude of the OF-HVDCC's terminal voltage (u_{abc} in Fig, 6) should be close enough to those

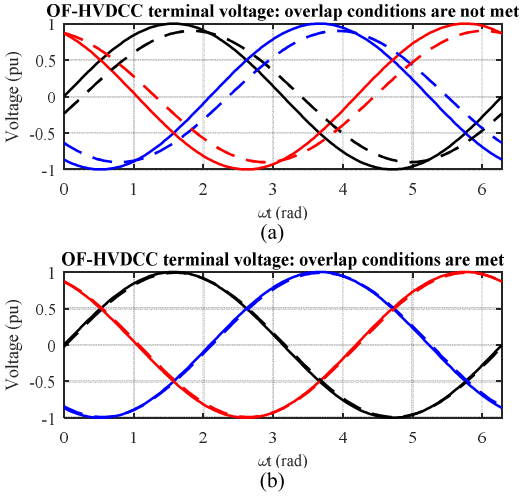

FIGURE 7. Illustration of the proposed overlap conditions for a smooth transfer between S3 and S1 operation states: (a) overlap conditions are not met and (b) overlap conditions are met (solid lines: voltage reference in the S1 operation mode, dashed lines: measured voltage in S3 operation state).

specified by the frequency reference unit, that resembles synchronization process, to attain a seamless state transfer, Fig. 7.

The resynchronization process will be started by specifying the i_d^* through a frequency controller as (4) to recover the OWF's frequency, measured by PLL (f_{LL}), to the reference

value specified by the frequency reference unit (f_r). However, the related i_d^* is bounded between $[i_{d0}, 0]$ for smooth system recovery purpose.

$$i_d^* = i_{d0} + \left(k_{pf} + \frac{k_{if}}{s}\right)(f_r - f_{LL}) \tag{4}$$

Once, the frequency recovers to an acceptable limit, an outer angle recovery controller will be activated to record the instantaneous difference between the θ_r (related to frequency reference unit) and θ_{PLL} (related to the PLL unit of the activated grid feeding mode) as $\Delta\theta_{rPLL0} = \theta_r - \theta_{LL}$. The recorded $\Delta\theta_{rPLL0}$ will be subtracted from the instantaneous θ_r and hence the predefined angle recovery criterion will be satisfied immediately. Note that, the voltage amplitude recovery is already ensured by the AC voltage control loop which is active in S2 and S3 states. Ultimately, the operation state will be returned to S1 in a seamless fashion once all the overlap conditions are met. Nevertheless, for seamless transition purpose, the integrator states of each module are appropriately initialized, Fig. 6, with the information recorded regarding the related variables from the last operating state and considering the proportional part of the controllers and feedforward terms.

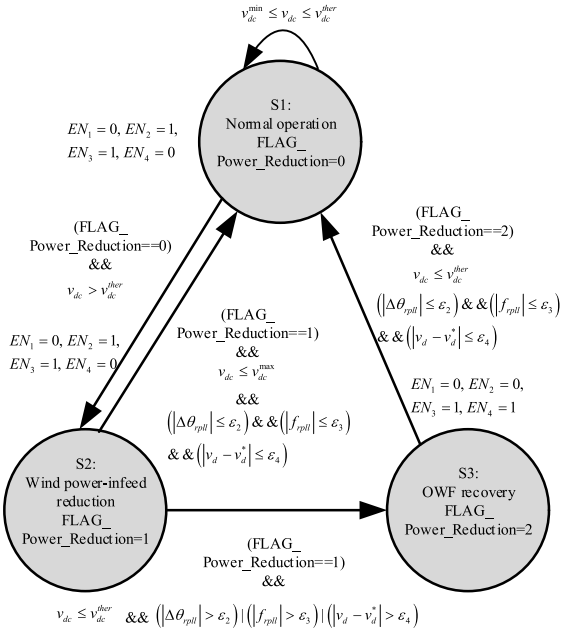

FIGURE 8. Proposed state machine to coordinate the operation of the OF-HVDCC between normal, wind power-infeed reduction, and OWF recovery operation states ($v_{dc}^{min} = 0.9$ pu, $\varepsilon_2 = \varepsilon_3 = \varepsilon_4 = 0.005$).

IV. MODELING AND CONTROL OF TYPE-4 WTGs

A. SYNCHRONIZATION POWER CONTROL CONCEPT

The SPC is a digital emulation of the simplified electrical and electromechanical characteristics of a synchronous generator, Fig. 9. It includes five critical units, namely PLC, RPLC, VCO, virtual admittance, current controller, and current modulus limiter [27]–[29].

The PLC unit generates a suitable differential virtual frequency ($\Delta\omega_s$) by processing the regulation error between the reference and measured active power $\left(P_g^* - P_g\right)$ and regulates the VSC's active power. Accordingly, the differential angle between the virtual back-EMF and grid voltage ($\mathbf{E}$ and $\mathbf{v}_g$) will ensure grid synchronization. The basic swing equation of (5) is employed to realize PLC with predefined inertia constant (H_v) and damping coefficient (D_v):

$$P_g^* - P_g = 2H_v\frac{d\omega_s}{dt} + D_v\left(\omega_s - \omega_g\right) \tag{5}$$

where ω_g denotes grid frequency at the point of voltage measurement that is measured by a PLL to reflect the effect of SGs damping winding effect accurately. Meanwhile, the differential magnitude of virtual back-EMF voltage (ΔE) is produced by the PI-based RPLC through regulation of reactive power setpoint (Q_g^*):

$$\Delta E = \left(K_{pq} + \frac{K_{iq}}{s}\right)\left(Q_g^* - Q_g\right) \tag{6}$$

Suitable feedforward terms including base grid frequency (ω_b) and voltage magnitude are included to obtain final E and ω_s values related to $\mathbf{E}$. The VCO unit generates the $\mathbf{E}$ in the three-phase stationary frame by the prepared data.

On the other hand, the derivative-free virtual admittance (X_v) (comprised of virtual inductance (L_v) and virtual resistance (R_v)) is easily emulated by generating/tracking a suitable reference for the current vector ($\mathbf{i}_g^*$) in the $\alpha\beta$ domain. Thanks to the high bandwidth of the PR regulator-based and robust current control loop, that does not need accurate phase angle information, the SPCs output electrical performance will be dictated by the virtual admittance block.

The exchanged P_g and Q_g can be easily changed similar to a synchronous generator by regulating the angle and amplitude of the $\mathbf{E}$ under the sufficiently inductive external grid. However, appropriate tuning for the control parameters are necessary to emulate a typical synchronous generator ($H_v = 5, X_v = 0.2$) with the desired damping ratio ($\xi_v = 0.8$) and resist against electrical resonances ($R_v = 0.05$, $D_v = 4H_v\xi_v\omega_n$, $\omega_n = sqrt\,(\omega_b/(2H_vX_v))$) [30].

B. PROPOSED VSG-BASED CONTROL STRUCTURE

Typical structure of a 5 MW cylindrical pole PMSG-based WTG is depicted in Fig. 9. It also includes the control modules for the MSC and the proposed control structure for the GSC and blade pitching unit. In this proposal, the GSC incorporates the SPC concept as the core controller and ensures MPPT by adopting the optimum P_g^* versus WTG rotor speed (ω_t) curve: ($P_g^* - \omega_t^3$). A supplementary droop-based $P_g^* - \omega_g$ controller is also employed to reduce the P_g^* during OWF ACC network frequency rise according to German GC ($k_{P\omega} = 20$):

$$P_g^* = \omega_t^3\left(1 - k_{P\omega}\left(\omega_g - 1\right)\right) \tag{7}$$

Considering the reactive channel of the GSC, a droop based $Q_g^* - V_g$ control scheme is implemented as (8) to

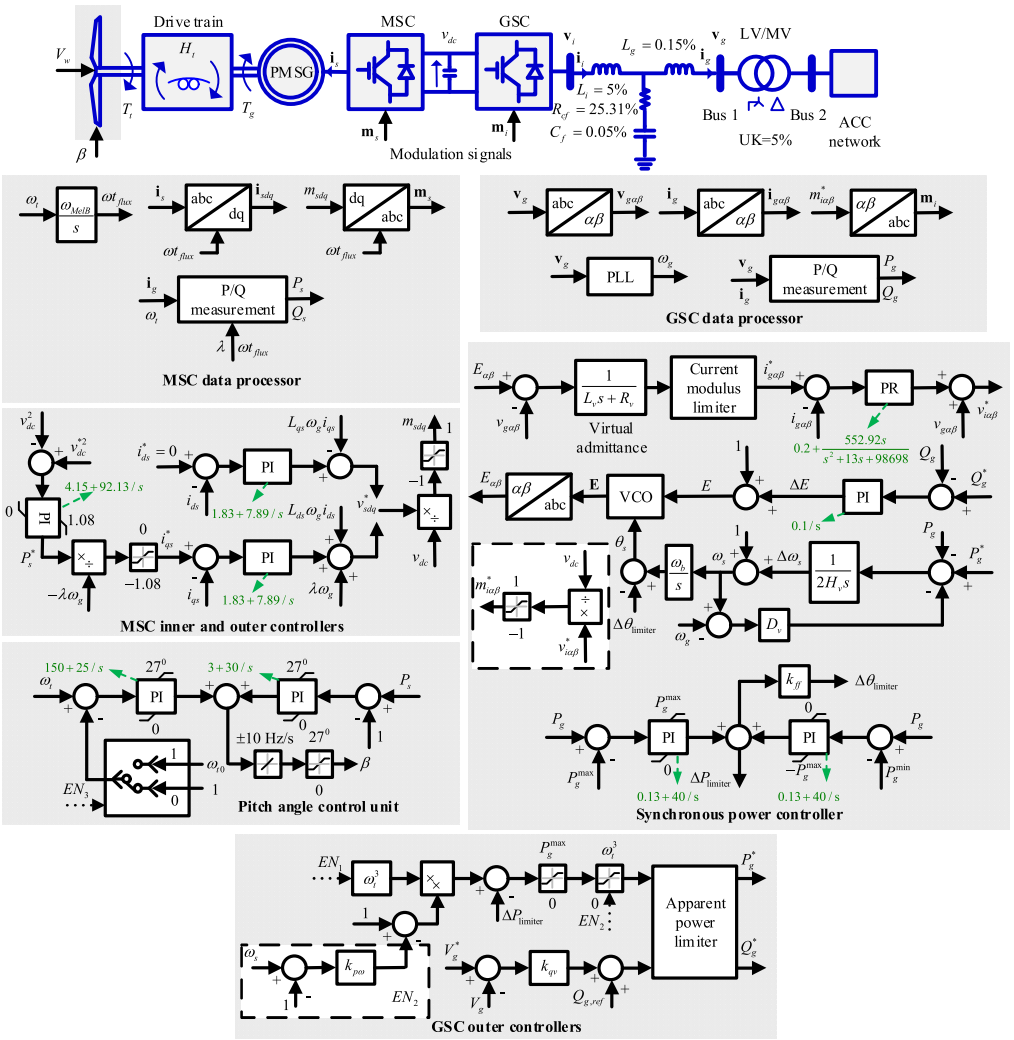

FIGURE 9. Typical establishment of VSG-controlled PMSG-based WTG as well as proposed control modules for MSC, GSC, and pitch unit ($\omega_{MelB} = 2\pi \times 34.3$ rad/s, $\omega_b = 2\pi \times 50$ rad/s, $v_{dc}^* = 1.21$ pu, $P_g^{min} = 0$ pu, $P_g^{max} = 1.08$ pu).

support/stabilize the ACC network's voltage in a coordinated fashion and equip the WTGs with the sufficiency of islanded operation/grid forming.

$$Q_g^* = Q_{g,ref} + k_{qv}(V_g - V_g^*) \tag{8}$$

in which k_{qv}, V_g, and $Q_{g,ref}$ represent the droop slope, network's voltage amplitude, and reactive power setpoint respectively (here: $Q_{g,ref} = 0$, $k_{qv} = 20$, and $V_g^* = 1$). The employed virtual inertia within the grid former SPCs is enabled after a sudden system generation/load imbalance and confines the RoCoF to enhance power system stability in the first few seconds. Also, the embedded $P_g^* - \omega_g$ droop characteristic stabilizes the ACC network's frequency deviation within a limited band by the provision of primary frequency response.

On the other hand, the MSC stabilizes the intermediary DC-link voltage (v_{dc}) by utilizing the WTG's kinetic energy as the main enabling energy source. As the SPC features a low-bandwidth PCL for inertia provision, v_{dc} control by the GSC is not feasible. So, v_{dc} control is done through specifying/tracking of an appropriate q-axis PMSG current within the adopted RFO control framework, $i_{qs}^* = -P_s^*/(\omega_t \lambda_s)$. PMSG current/torque and active power limitations are also catered while taking $i_{ds}^* = 0$ to minimize copper losses. Accordingly, stator voltage signals are generated by the employed RFO control.

Finally, the total sum of two pitch compensation and control modules determines the pitch angle value, Fig. 9. In more details, the role of confining the ω_t to its maximum value is assigned to the pitch control loop. On the other hand, limitation of the PMSG's active power below the rated maximum value is dedicated to the pitch compensation loop. Nevertheless, the operation of the WTG below the rated wind speeds implies zero steady-state blade angle value as for the MPPT process.

C. PROPOSED STATE MACHINE FOR PRIMARY FREQUENCY RESPONSE COORDINATION

The proposed state machine, Fig. 10, projects to coordinate the operation of the WTG between S1, S2, and S3 operation

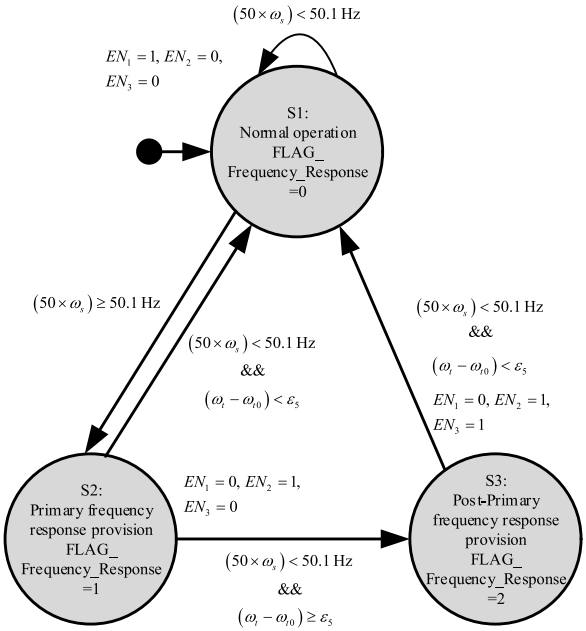

FIGURE 10. Proposed state machine to coordinate the operation of the individual WTGs between normal, primary frequency response provision, and post-primary frequency response provision states ($\varepsilon_5 = 0.01$).

states that are defined in Fig. 10. Once the ACC network frequency ($50\times\omega$s) exceeds $50\times\omega_{s,\max} = 50.1$ Hz, the WTG will be switched to operate in the S1 state. This will be occurred as a result of the proposed wind power-infeed curtailment, through the control mechanism related to the operation of the OF-HVDCC in S2 state of Fig. 8, in response to an onshore network AC fault. In S2 operation state of Fig. 10, the WTG will decrease its output electric power according to the droop characteristic of (7). However, ω_t signal in (7) is frozen to ω_{t0}, the last recorded value of the ω_t in S1, to ensure accurate active power reduction. A dynamic limiter is also activated to confine the P_g^* to the available wind power (ω_t^3) while operating in S2 and hence avoid excessive speed drop of the WTG. This instability might appear during the post-fault period in which the OWF's active power is ramped up by the OF-HVDCC while the wind speed is decreased during the long transient state implied by the low ramping rate specified in S4 of Fig. 5 for the ON-HVDCC. In the S2 state, the WTG will start to accelerate until the rated WTG rotor speed value is reached due to the below MPPT value of P_g. Afterward, the pitch angle control loop, Fig. 9, will effectively regulate the ω_t to its maximum value by pitching the WTG blades. In other words, the WTG's aerodynamic de-loading under low and medium wind speed conditions is done by WTG over-speeding as much as possible and then the pitching action is utilized and hence reduced wear and tear will be achieved in the WTG's blades. Nevertheless, wind speed decrease during a long transient state impacts the described process with certain dynamics. However, under the over-rated wind speeds (WTG's constant power region) the pre-FRT WTG's speed is already regulated to its nominal value by the pitch control loop. Accordingly, pitching action will be solely employed for the aerodynamic de-loading purpose.

As soon as $50\times\omega_s < 50\times\omega_{s,\max}$ condition holds, the WTG's operation state will be switched to the S3 state given that $(\omega_t-\omega_{t0})>\varepsilon_5$. In this state, the ω_t^* for the pitch angle control loop is changed to ω_{t0} to aid smooth power system recovery ($EN_2 = 1$) and finally switch back to the S1 state. It is noted that if $(\omega_t-\omega_{t0})\leq\varepsilon_5$ condition holds at the ACC network's frequency recovery instant, the WTG's operation state will be directly switched to the S1 state: ($EN_1 = EN_0 = 0$). This can mainly occur under wind speed decrease condition during a prolonged transient state in which the dynamic P_g^* limiter already confines the P_g to ω_t^3. Upon switching to S1, the WTG starts to increase the generated active power smoothly by the action of MPPT if the wind speed is increased during the long transient period. However, constant wind speed under a short transient period is the most expected condition in which the WTG will generate its pre-fault power finally.

V. TRANSIENT ACTIVE POWER REDUCTION SHARING ANALYSIS

The reduced $\Delta P_{cur.}$ will be shared between the OWF's WTGs considering three time intervals including important first few power cycles, transient state, and steady-state. Load sharing characteristics are of high importance under the impacts of the wind wake effect that is modeled by the widely adopted, simple, and accurate Park's multiple wake model [22].

A. FIRST FEW POWER CYCLES PERIOD

Regarding this time interval, the PLC and RPLC in Fig. 9 are low-bandwidth controllers within the electromechanical time scale. Accordingly, the angle (θ_s) and amplitude (E) of the virtual back-EMF voltage (**E**) can be effectively considered to be constant. However, the current control loops are usually fast enough for effective virtual admittance emulation. Hence, the load sharing characteristics will be dominated by ACC network's impedances including virtual admittances, LV/MV transformers, and internal cablings. Fig. 11 shows the resultant equivalent circuit to study/estimate the initial load sharing in fundamental frequency according to practical data of [22] that are presented in WTG per-unit base (5 MW, 3 kV, and 50 Hz). From Fig. 11, it is obvious that the internal cabling parameters are much less than other OWF's actual and virtual impedances and hence internal cabling can be effectively neglected in the analyzes. Also, under the selected X_v and R_v parameters the system is inductive enough to realize effective P/Q decoupling. Moreover, this system has relatively short (virtual/actual) transmission lines, i.e., a small phase angle change can result in large active power change. Thus, the power flow from each WTG to collection bus in Fig. 11 (P_{ijcb}) can be approximated and linearized as (9) and (10) respectively:

$$P_{ijcb} = \frac{E_{ij}E_{cb}}{X_{vij}+X_{Tij}}\sin\left(\delta_{ij}-\delta_{cb}\right) \tag{9}$$

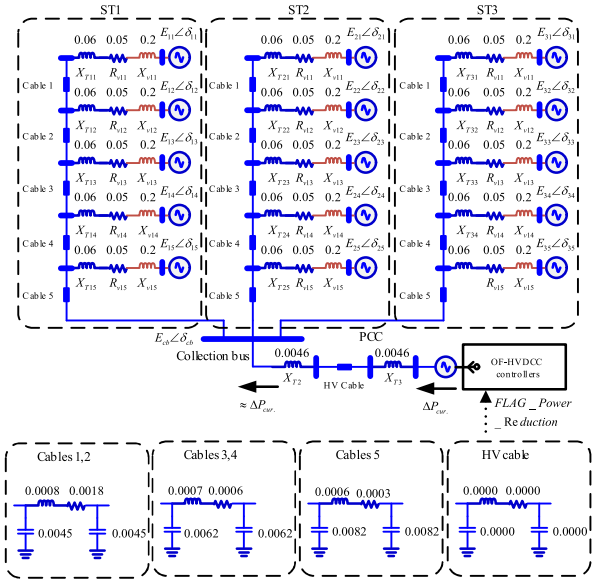

FIGURE 11. Proposed equivalent circuit to investigate the fundamental frequency negative load sharing in the first few power cycles.

$$\Delta P_{ijcb} = \frac{E_{ij}E_{cb}}{X_{vij}+X_{Tij}}\cos\left(\delta_{ij0}-\delta_{cb0}\right)\Delta\left(\delta_{ij}-\delta_{cb}\right) + \frac{E_{ij}}{X_{vij}+X_{Tij}}\sin\left(\delta_{ij0}-\delta_{cb0}\right)\Delta E_{cb} \tag{10}$$

Also, i and j symbols are related to j-th WTG in i-th string and other symbols are shown in Fig. 11. Regarding the stated assumptions/findings, it is accurate enough to derive $\Delta P_{ijcb}/P_{ijcb0}$ ration from (9) and (10) as below:

$$\frac{\Delta P_{ijcb}}{P_{ijcb0}} = -\frac{\cos\left(\delta_{ij0}-\delta_{cb0}\right)}{\sin\left(\delta_{ij0}-\delta_{cb0}\right)}\Delta\delta_{cb} \tag{11}$$

Once the OWF's active power is reduced by the OF-HVDCC, certain positive phase angle jump ($\Delta\delta_{cb}$) will be induced instantly to force the multi-VSG system to reduce its injected power immediately. According to (11), upstream WTGs will inject more active power and hence will have higher δ_{ij0} values and lower cot $\left(\delta_{ij0}-\delta_{cb0}\right)$ values compared to downstream WTGs. Accordingly, downstream WTGs will feature an undesirable higher absolute $\Delta P_{ijcb}/P_{ijcb0}$ ration despite their lower initial wind power that characterizes poor transient power-sharing.

1) PROPOSED METHODS TO IMPROVE TRANSIENT NEGATIVE LOAD SHARING

It is proposed to tune WTGs X_{vij} values to attain uniform identical load angle $\left(\delta_{ij0}-\delta_{cb0}\right)$ for OWF's WTGs. To do so, pre-fault PF equations of the OWF's ACC network should be developed considering the slack bus role of OF-HVDCC in Bo-C2 bus of Fig. 3, the proposed equivalent circuit of Fig. 11, measured active power of individual WTGs at Bus1 of Fig. 9, and the role of implemented $Q_g^*-V_g$ droop controllers of (7). As the active/reactive powers of the individual WTGs are measured at Bus1 of Fig. 9, the adopted X_{vij} values will not impact the PF results. From PF results (P_{gij0}, Q_{gij0}, $V_{Bus1ij,0}$, $\delta_{Bus1ij,0}$), the δ_{ij0} and E_{ij0} of the WTGs virtual back-EMF voltage can be computed from (12) and (13).

$$P_{gij0} = \frac{E_{ij0}V_{Bus1ij,0}}{X_{vij}}\sin\left(\delta_{ij0}-\delta_{Busij1,0}\right) \tag{12}$$

$$Q_{gij0} = \frac{V_{Bus1ij,0}}{X_{vij}}\left(E_{ij0}-V_{Bus1ij,0}\right) \tag{13}$$

To calculate suitable X_{vij} values, the X_{vij} value related to the most upstream (base) WTG is taken to be $X_{v0}=0.2$ pu at the first step. Accordingly, the related $\delta_{ij0}=\delta_{ijbase0}$ can be specified from (12) and hence $\left(\delta_{ij0}-\delta_{cb0}\right)$ load angle can be calculated considering PF results. Afterward, X_{vij} values of downstream WTGs can be calculated from (12) by considering uniform load angle of $\left(\delta_{ij0}-\delta_{cb0}\right)=\left(\delta_{ijbase0}-\delta_{cb0}\right)$. As a result, certain positive X_{vij} values will be assigned to downstream WTGs and uniform $\Delta P_{ijcb}/P_{ijcb0}$ ration will be approximately attained for OWF's WTGs.

The alternative remedy is to accept poor transient load sharing, but avoid motor mode operation of downstream WTGs under severe $\Delta P_{cur.}$ conditions while upstream WTGs are still in generator mode. In this regard, the APL proposed by [27] is implemented that projects to limit the VSG's active power between its typical minimum and maximum values (here: $P_{g,\min}=0$ pu and $P_{g,\max}=1.08$ pu). It is done by introducing $\Delta P_{\text{limiter}}$ and $\Delta\theta_{\text{limiter}}$, specified by two parallel PI controllers, as feedforward terms to VSG's active power reference and virtual angle respectively, Fig. 9. $k_{ff}=L_v/E_{nom.}V_{nom.}\cos\delta_{nom}$ where $E_{nom.}$, $V_{nom.}$, and δ_{nom} represent nominal $\mathbf{E}$ amplitude, nominal $\mathbf{v}_g$ amplitude, and nominal load angle respectively. Hence, the delivered active power will be effectively between $\left[P_{g,\min},P_{g,\max}\right]$ limit thanks to the action of $\Delta\theta_{\text{limiter}}$ in transient state and action of $\Delta P_{\text{limiter}}$ in the steady-state.

B. TRANSIENT STATE

In this time interval, the PLC controllers of the WTGs will share the negative load by OWF's frequency regulation. Each WTG projects to follow its predefined $P_g^*-\omega_g$ of (7) in steady-state; however, the slow PLC dynamics introduces certain dynamics beforehand. The PLC, RPLC, and filtering parameters mainly specify the period of this time interval. In this line, the downstream WTGs will experience the highest $\Delta P_{ijcb}/P_{ijcb0}$ ration until reaching the steady-state. One approach to improve the poor transient load sharing is to increase the PLC's bandwidth and hence reduce the transient period [31]. However, it still cannot impact the first few power cycles and it contradicts with the essential inertia provision function of the VSGs. Different frequency regulation characteristics of the WTGs is due to their different operating point under the wind wake effect and non-uniform load sharing that causes different driving power $\left(P_g^*-P_g\right)$ in the swing equation of (5). Hence, each VSG will experience slightly different virtual speed during the transient interval. The effective employed remedy is to assign an arbitrary H_v to the most

upstream WTG (here: $H_v = 5$) and calculate the related base P^*_{g0}/H_v ration considering that uniform $\Delta P_{ijcb}/P_{ijcb0}$ ration for entire WTGs is already ensured using the proposed virtual admittance tuning method. Accordingly, the H_v values related to the downstream WTGs should be tuned to ensure uniform P^*_{g0}/H_v ration for entire WTGs.

C. STEADY STATE

Finally, $\Delta P_{cur.}$ will be shared between OWF's WTGs according to $P^*_g - \omega_g$ of (7). This results in steady-state frequency rise of (14) and final WTGs power of (15) that exhibit uniform $\Delta P_{ijcb}/P_{ijcb0}$ ration for OWF's WTGs.

$$\Delta\omega_g = \frac{\Delta P_{cur.}}{\sum_{i=1}^{N2}\sum_{j=1}^{N_1} k_{p\omega ij}\omega^3_{t0ij}} \tag{14}$$

$$P^*_{gi} = \omega^3_{t0i}\left(1 - k_{p\omega i}\Delta\omega_g\right) = \omega^3_{t0i} \times \left(1 - k_{p\omega i}\frac{\Delta P_{cur.}}{\sum_{i=1}^{N2}\sum_{j=1}^{N_1} k_{p\omega ij}\omega^3_{t0ij}}\right) \tag{15}$$

VI. TIME DOMAIN SIMULATION RESULTS, PERFORMANCE EVALUATION, AND ANALYSIS

To evaluate the effective dynamic performance of the proposed onshore FRT strategy and its influence on the OWF and MT-HVDC grid levels, the test grid explained in Section II is considered. This test grid is simulated using EMT models of MATLAB/SIMULINK platform.

A. BALANCED FAULT

A 250 ms, 70% balanced voltage dip is introduced in $t = 0.1$ s using the controllable voltage source of A0 as the most severe FRT scenario. DC fault scenarios are out of the study scope [32], [33]. The entire OWFs WTGs experience over nominal wind speeds which are stated by the blue colors in Fig. 3 to maximize the challenge of onshore FRT. The key simulation results are presented in Fig. 12 in their desired time ranges. The severity of the fault and consequent fast positive sequence reactive current support by the ON-HVDCC, Fig. 12.c, reduces the corresponding transported power to zero, Fig. 12.d. As a result, direct voltages start to increase with a similar transient process in entire DC buses due to short HVDC line lengths, Fig.12.e. Direct over-voltages are intercepted by OF-HVDCCs and followed by a fast power curtailment command as per (2) after a certain delay in the order of milliseconds, Fig. 12.d and Fig 12.g. Hence, the wind power in-feed by both OF-HVDCCs is decreased to almost zero successfully within approximately 100 ms after fault inception. Thereupon, a new active power balance is established inside the MT-HVDC grid so that direct over-voltages are effectively confined below the maximum admissible value of 0.2 pu thanks to fast dynamics of direct wind power in-feed curtailment.

As a result of fast power curtailment, the OWFs frequency starts to accelerate gradually (Fig. 12.h). A limited RoCoF roughly below 4 Hz/s is visible thanks to the virtual inertia embedded in the individual WTGs PCL and employed control parameters under the base case. Meanwhile, OWFs voltage amplitude is maintained within acceptable limits, Fig. 12.f and Fig.12.h, which verifies effective grid forming capability of SPC controlled WTGs despite the impacts of OWFs inductive elements. The curtailed power is stored as kinetic energy in the WTGs rotating masses due to the power balance imposed by each WTGs MSC, Fig. 12.i and Fig. 12.j. The speed increase takes the limited value of 0.03 pu mainly due to relatively large rotating masses and the action of the pitch angle controllers, Fig.12.i.

After the onshore AC fault clearance, the operation state of the ON-HVDCC is switched to the S1 in Fig. 5 and hence the restoration process is started (the ramp-up process is neglected to reduce simulation time). Accordingly, the related direct voltage controller regulates the Bm-A1 bus's direct voltage to its pre-defined setpoint, Fig. 12.e. Finally, the transmitted active power is reached to the related pre-fault value and the Bm-A1 bus's direct voltage is successfully stabilized. Smooth power system restoration is obvious thanks to the employed state machines that is beneficial for whole system stability.

Regarding the Cm-C1 OF-HVDCC, the related operation state is switched to the S3 in Fig. 8 in turn since the Bm-C1 bus's direct voltage is reached below 1.05 pu, Fig. 12.e. Considering Fig. 12. g, the OF-HVDCC's active current returns itself to the related pre-fault value and evolutes in subsequent seconds under the influence of OWF's recovery process explained in Section III.B.1. After successful recovery process of the OWF, the OF-HVDCC's operation state is switched from S3 to S1 in a seamless manner in $t = 10.21$ s, Fig. 12. g.

B. UNBALANCED FAULT

A 250 ms, 80% phase a to ground voltage dip is introduced in $t = 0.1$ s. Since there is still significant remaining current capacity in the ON-HVDCC to transmit active power, the appeared DSF ripple-free direct over-voltage phenomenon (below the 1.11 pu) in Fig. 13.e is much less than that's related to the balanced fault scenario. As the switching criterion defined for the OF-HVDCCs in Fig. 8 (to activate the S2 operation state) is met, the act of direct wind power-infeed reduction is performed similar to the case of a balanced fault, Fig. 13.d and Fig.13.f. Less severe appeared direct over-voltage, compared to the balanced fault scenario, implies that the functionality of proposed onshore FRT control strategy is beneficial to reduce electrical stresses on MT-HVDC network installations rather than failure prevention.

C. SENSITIVITY ANALYSIS

The onshore unbalanced FRT scenario of Section VI.B is simulated again with two different sets of k_{PC} (case A) and H_v (case B) parameter values applied to distinct OWFs

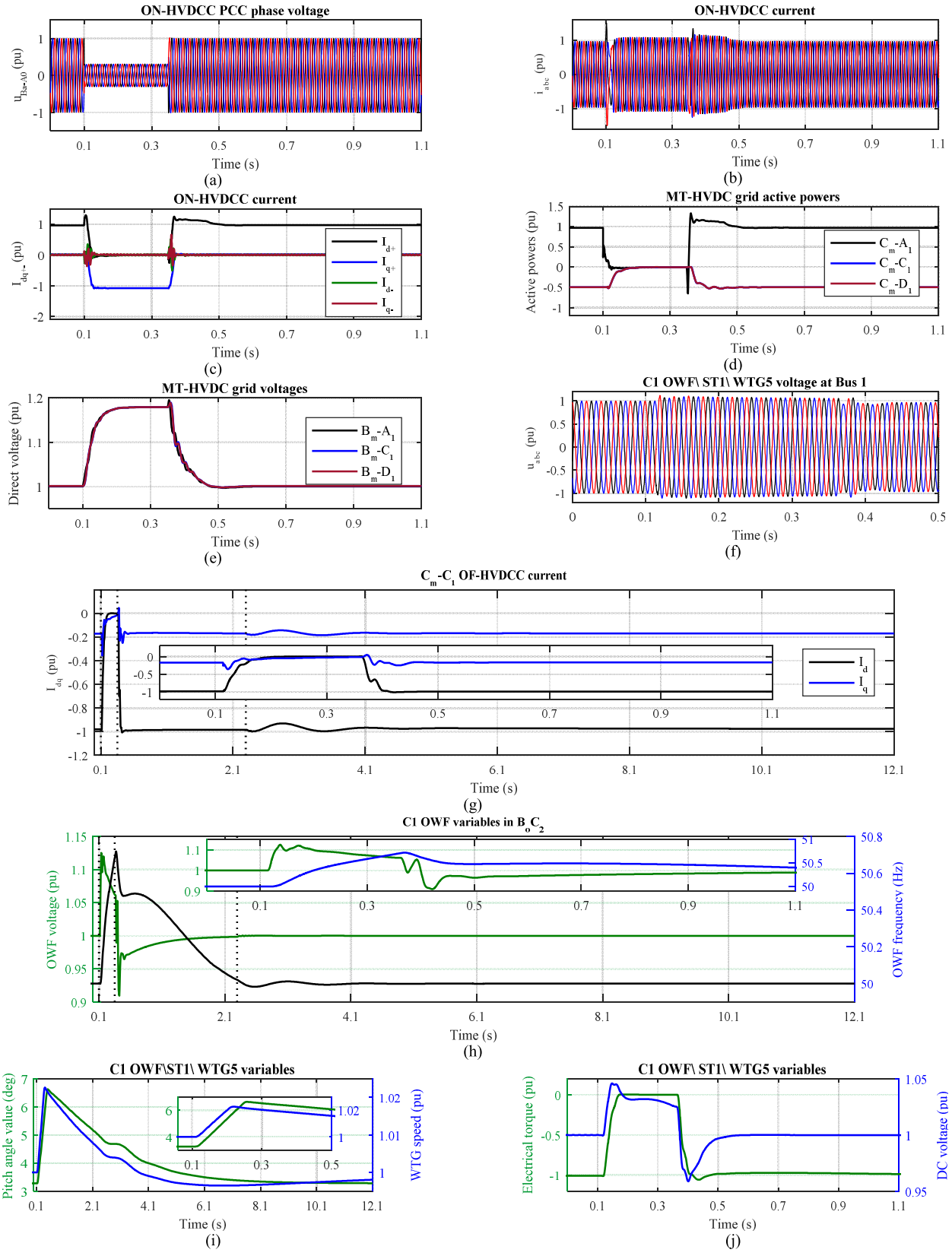

FIGURE 12. Time-domain simulation results for the proposed onshore FRT strategy during balanced fault.

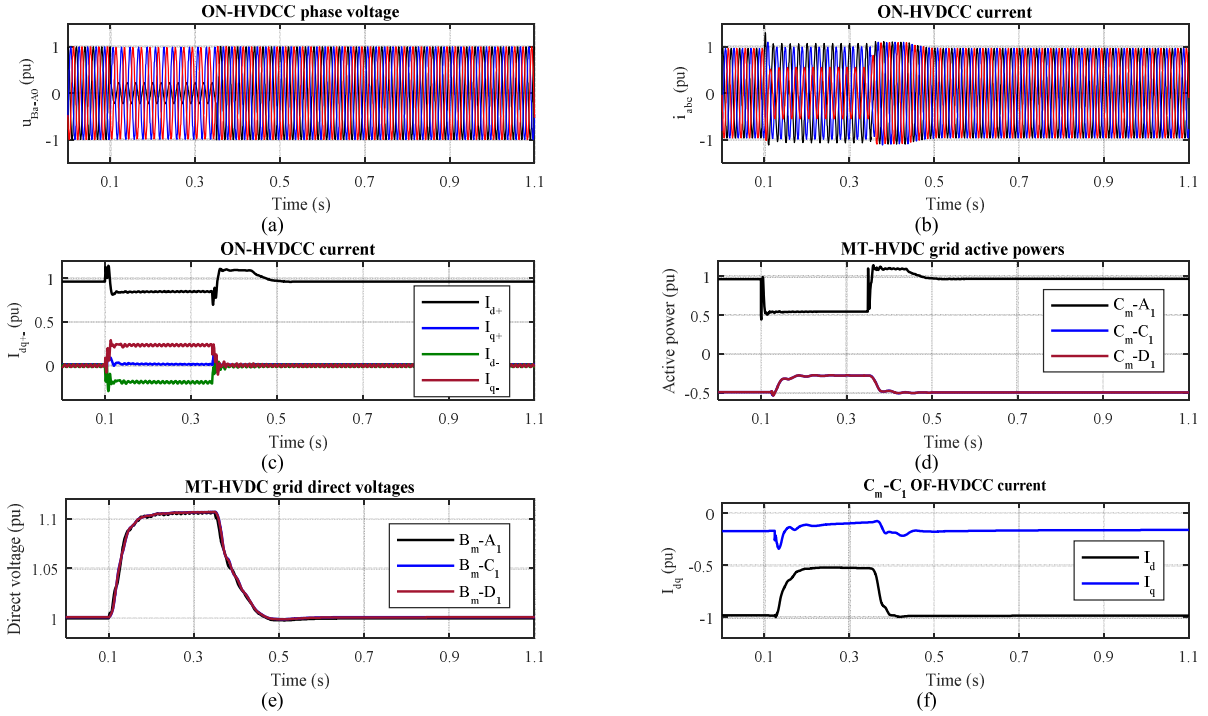

FIGURE 13. Simulation results for the proposed onshore FRT strategy during unbalanced fault.

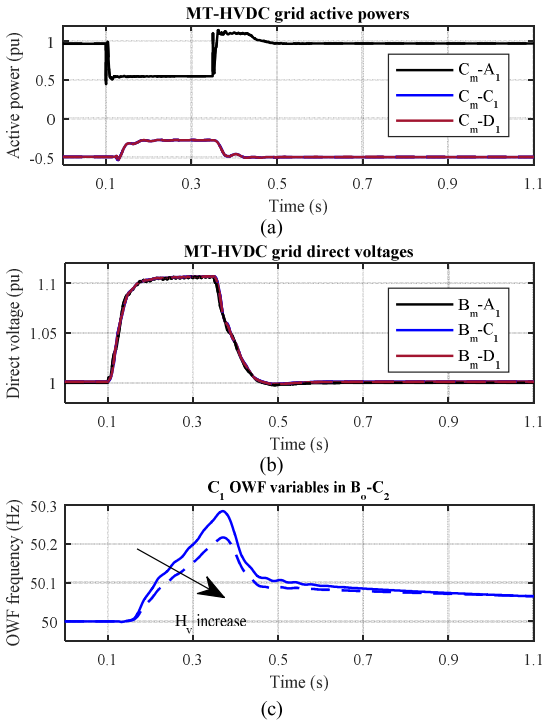

FIGURE 14. Simulation results for the proposed onshore FRT strategy under different values of Hv during onshore unbalanced fault (solid lines: Hv = 5 for entire WTGs in both C1 and D1 OWFs, dashed lines: Hv = 8 for entire WTGs in C1 OWF and Hv = 5 for entire WTGs in D1 OWF).

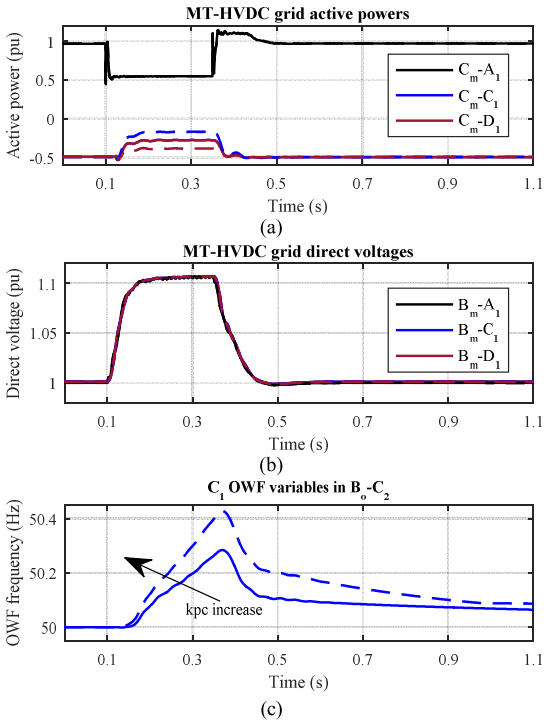

FIGURE 15. Simulation results for the proposed onshore FRT strategy under different values of kpc during onshore unbalanced fault (solid lines: kpc = 1/(0.13) for both C1 and D1 OWFs, dashed lines: kpc = 1.5/(0.13) for C1 and OWF and kpc = 0.5/(0.18) for D1 and OWF.

WTGs and OF-HVDCCs as stated in Fig. 15 and Fig. 14. Possible applications are to adjust the wind power curtailment share between OWFs and shape the influence of fast wind power in-feed curtailment on OWFs in terms of RoCoF. Considering Fig. 14. a, it is found that the variation of H_v does not influence the fast wind power in-feed curtailment and related shares and hence the transient over-voltage is still mitigated effectively, Fig.14. b. It is mainly since the

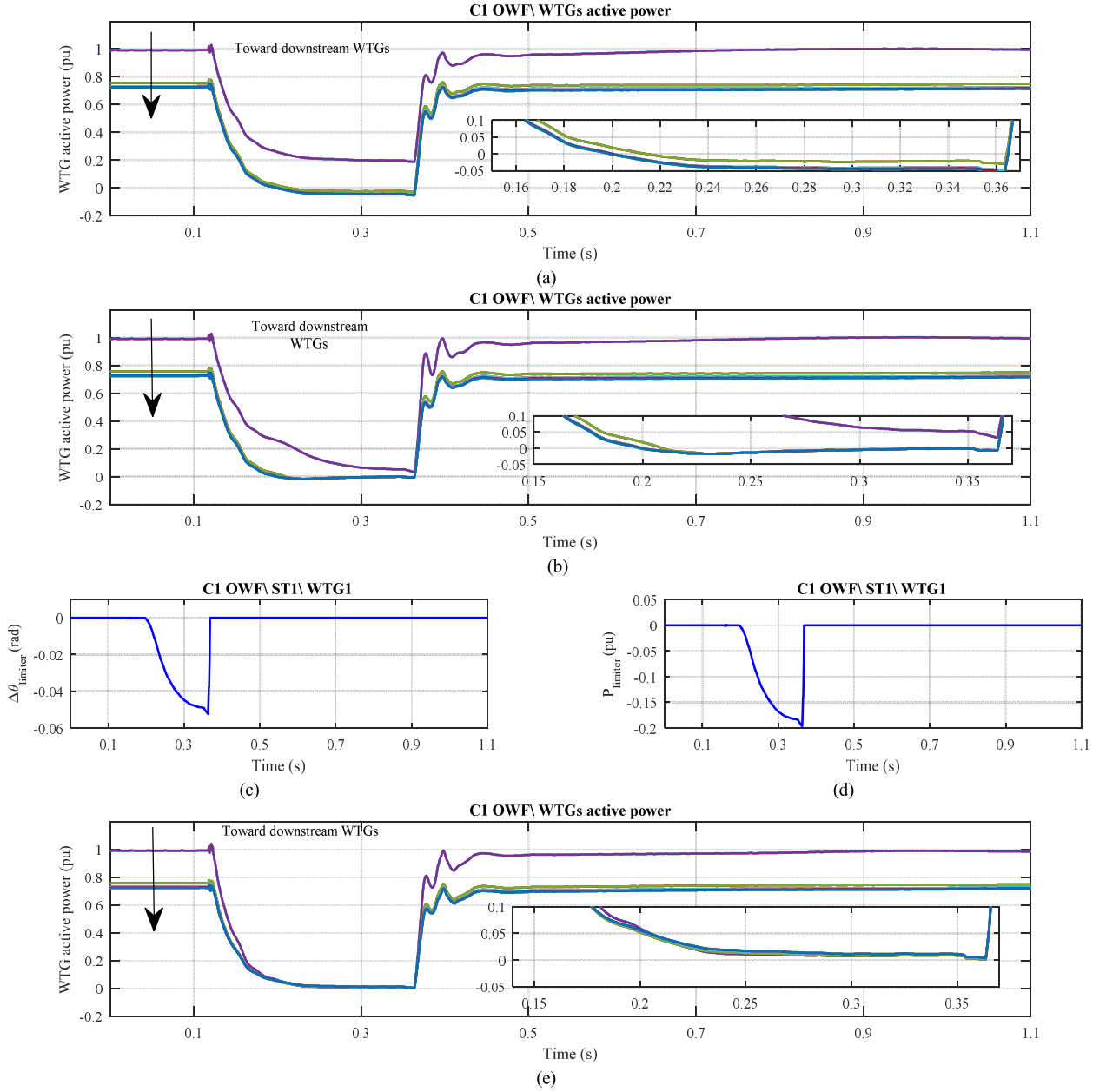

FIGURE 16. Simulation results for the proposed onshore FRT strategy under wind wake effect. (a) Without any transient negative load sharing improvement measure, (b-d) Employing the APL units, (e) employing the proposed virtual admittance tuning method (Xv = 0.2 pu for WTG5 in all strings, Xv = 0.2811 pu for WTG4 in all strings, Xv = 0.2911 pu for WTG3 in all strings, Xv = 0.2923 pu for WTG2 in all strings, Xv = 0.2932 pu for WTG1 in all strings).

power curtailment is performed by the OF-HVDCCs directly, hence, the WTG dynamics hardly affects the dynamics of power curtailment process under preserved OWF stability. Moreover, H_v increase reduces OWFs RoCoF which decreases the OWFs stress and prevents tripping of the anti-islanding detection relays, Fig. 14. c. Nonetheless, very high values of H_v might danger the main objective of MPPT by reducing the bandwidth of the SPC's PCL under normal operation.

On the other hand, the burden of wind power in-feed curtailment can be distributed among different OWFs by appropriate selection of k_{PC} values while still reducing the wind power in-feed effectively by the entire OF-HVDCCs, Fig. 15. a, and hence avoiding transient direct overvoltages, Fig. 15. b. Nevertheless, it is clear from Fig. 15. c that the increased k_{PC} value (here in C1 OWF) implies deeper active power curtailment and hence higher frequency increase in terms of RoCoF.

D. IMPACTS OF THE WIND WAKE EFFECT

To investigate the impacts of the wind wake effect, the balanced fault condition of Section VI.A is simulated again,

however, the WTGs in both OWFs operate in MPPT region following the wind speeds tabulated in green colors in Fig. 3. The key results are summarized in Fig. 16. From Fig. 16. a, the poor transient active power sharing is evident as upstream WTGs (WTG5 in all strings of Fig. 3) experience the lowest $\left|\Delta P_{ijcb}/P_{ijcb0}\right|$ ration of 0.815 while the most downstream WTGs (WTG1 in all strings) experience $\left|\Delta P_{ijcb}/P_{ijcb0}\right|$ of 1.055. Hence, downstream WTGs enter in the motor region due to the severe wind power-infeed curtailment while the upstream WTGs are still in generator region that is not acceptable. In this regard, the APL described in Section V.A.1 is implemented. From Fig. 16. b, it is evident that the action of APLs by the transient increase of virtual back EMF's angle, Fig. 16. c, and active power reference, Fig.16. d, has effectively prevented the motor mode operation of the downstream WTGs. Moreover, it is still evident from Fig. 16. b that $\left|\Delta P_{ijcb}/P_{ijcb0}\right|$ ration is not still equal for all WTGs. Finally, fast virtual angle change implies a very abrupt increase in virtual back EMF's frequency. Considering the grid forming action of WTGs, this will increase the burden on entire OWFs PLL units to relock.

In this vein, the proposed virtual admittance tuning method is applied and hence almost identical $\left|\Delta P_{ijcb}/P_{ijcb0}\right|$ ration of 0.98 is achieved for entire WTGs without opting for additional APLs, Fig. 16. e. The assignment of larger virtual admittances to downstream WTGs to attain almost identical pre-fault $\left(\delta_{ij0}-\delta_{cb0}\right)$ value is clear from Fig. 16's caption. Nevertheless, this method is OWF friendly in comparison to APL based method as no fast virtual angle change will be applied.

E. COMPARATIVE SIMULATIONS

Two available FD-PSACR and PSVD-PSACR based FRT control strategies are also simulated to establish comparative simulations [14], [20]. The key results are summarized in Fig. 17 and Fig. 18 under the balanced onshore fault condition of Section VI.A. It is clear that the transient direct over-voltage has successfully triggered the strategies in place by a transient increase in the C1 OWF's frequency reference up to 52.5 Hz (Fig. 18.c) and a transient decrease of its voltage amplitude down to 0.5 pu (Fig. 17.c). The magnitudes of the controlled voltage drop and frequency increase are dependent on the designed proportional constants of the FD-PSACR and PSVD-PSACR loops. However, the applied voltage dips might still violate the permissible FRT envelope of the WTGs mainly when the slow recovery process is intended by opting for S4 in Fig. 5. The rapid frequency excursion and controlled voltage reduction are absent in the proposed FRT control strategy (Fig. 12. h) which is a significant improvement. The fast FRT positive sequence reactive current injection of the WTGs are deactivated as it tries to attenuate the intentionally applied voltage drop. Also, it might destabilize HVDC connected OWF due to the absence of a physical short circuit fault. This indicates an apparent interference between the requirements for OWF physical balanced faults and controlled OWF voltage drop. Hence, PSVD reactive

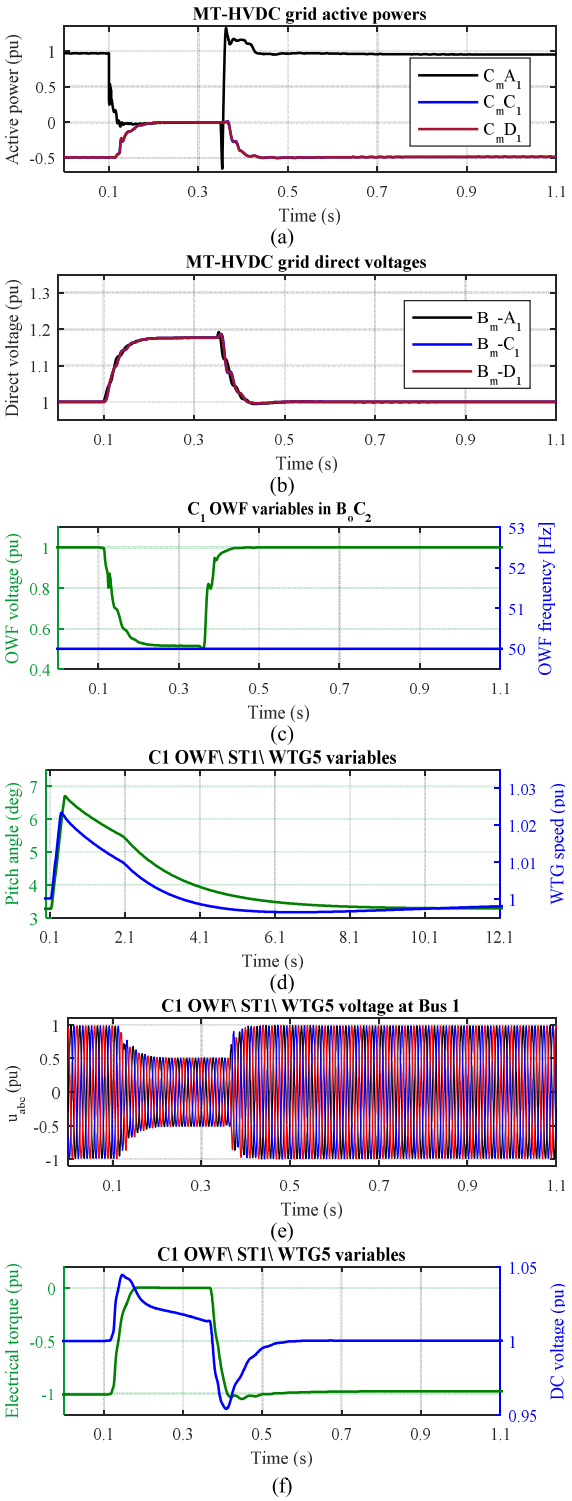

FIGURE 17. Simulation results for the voltage modulation based onshore FRT strategy during balanced fault.

current support should be provided only for the voltage drops deeper than the maximum envisioned controlled voltage drop. Such interference does not exist when the proposed method is employed as no controlled voltage reduction will be applied.

Upon excitation of the WTGs inertial and primary responses, the exported wind power is quickly reduced as

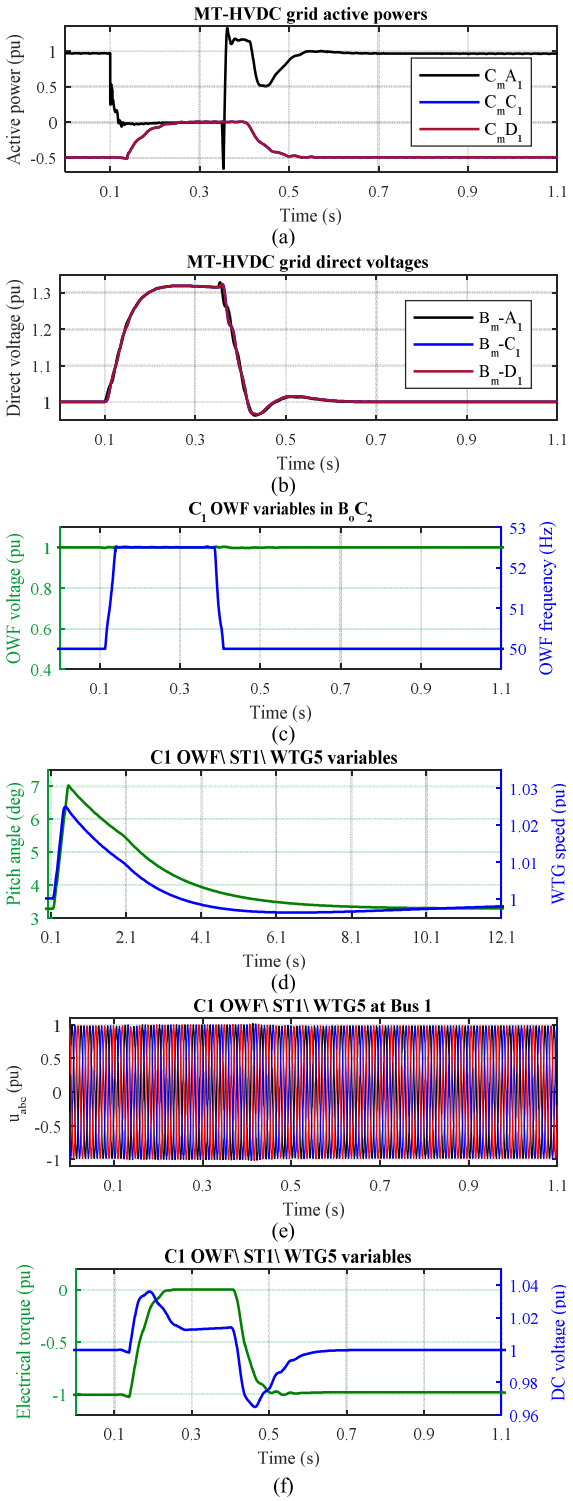

FIGURE 18. **Simulation results for the frequency modulation based onshore FRT strategy during balanced fault.**

a result of the coordinated control rules implemented on the WTGs GSC and the OF-HVDCC. As expected, the frequency modulation approach has failed to confine direct over-voltages to the value of 0.2 pu, Fig. 18. b, due to the frequency measurements delays. The results shown are already optimistic since the limited permissible RoCoF limitation is disabled in the OF-HVDCCs control unit. On the other hand, the voltage modulation approach has limited the direct over-voltages to 0.2 pu thanks to the possibility of easy voltage measurements and fast WTGs current control loops, Fig. 17. b. Similar results are obtained regarding the establishment of a new active power balance and the storage of the imbalance power on the WTGs rotating masses.

VII. CONCLUSION

In this research, a new communication-free control strategy was proposed in OWF level based on the well-tailored VSG concept. It was to enhance the FRT grid code compliance of the MT-HVDC grid connected to the onshore AC network through fast and direct reduction of the injected wind power by OF-HVDCCs. A set of state machines were also proposed to coordinate the operation of the entire power system including HVDC converters, individual Type-4 WTGs, etc. in a smooth fashion. Furthermore, a virtual impedance tuning method and an APL scheme were proposed to enhance transient load sharing between OWFs WTGs.

Based on performed simulations, the successful dynamic performance of the proposed FRT control strategy was shown in terms of containing direct over-voltages below the technical limit under various onshore AC network (balanced and unbalanced) FRT conditions and smooth post-fault power system recovery. Also, minimized stress was imposed to OWFs ACC network in terms of limited RoCoF and not performing controlled voltage reduction and hence OWFs tripping risk is minimized. In addition, it was concluded that by appropriate selection of control parameters, the burden of wind power in-feed curtailment can be distributed among different OF-HVDCCs and the impacts on OWF levels can be influenced. Finally, it was also observed that employing proper virtual impedances (and APL scheme to a certain extent) can substantially improve the load sharing between OWFs WTGs.

REFERENCES

[1] A. Kirakosyan, M. S. E. Moursi, and V. Khadkikar, "Fault ride through and grid support topology for the VSC-HVDC connected offshore wind farms," *IEEE Trans. Power Del.*, vol. 32, no. 3, pp. 1592–1604, Jun. 2017.

[2] M. Asif, H.-Y. Lee, U. A. Khan, K. Park, and B. W. Lee, "Analysis of transient behavior of mixed high voltage DC transmission line under lightning strikes," *IEEE Access*, vol. 7, pp. 7194–7205, 2018.

[3] A. Moawwad, M. S. El Moursi, and W. Xiao, "Advanced fault ride-through management scheme for VSC-HVDC connecting offshore wind farms," *IEEE Trans. Power Syst.*, vol. 31, no. 6, pp. 4923–4934, Nov. 2016.

[4] A. Moawwad, M. S. El Moursi, W. Xiao, and J. L. Kirtley, "Novel configuration and transient management control strategy for VSC-HVDC," *IEEE Trans. Power Syst.*, vol. 29, no. 5, pp. 2478–2488, Sep. 2014.

[5] A. Moawwad, M. S. El Moursi, and W. Xiao, "A novel transient control strategy for VSC-HVDC connecting offshore wind power plant," *IEEE Trans. Sustain. Energy*, vol. 5, no. 4, pp. 1056–1069, Oct. 2014.

[6] I. Erlich, C. Feltes, and F. Shewarega, "Enhanced voltage drop control by VSC–HVDC systems for improving wind farm fault ridethrough capability," *IEEE Trans. Power Del.*, vol. 29, no. 1, pp. 378–385, Feb. 2014.

[7] B. Silva, C. L. Moreira, H. Leite, and J. A. P. Lopes, "Control strategies for AC fault ride through in multiterminal HVDC grids," *IEEE Trans. Power Del.*, vol. 29, no. 1, pp. 395–405, Feb. 2014.

[8] X. Hu, J. Liang, D. J. Rogers, and Y. Li, "Power flow and power reduction control using variable frequency of offshore AC grids," *IEEE Trans. Power Syst.*, vol. 28, no. 4, pp. 3897–3905, Nov. 2013.
[9] O. D. Adeuyi, M. Cheah-Mane, J. Liang, L. Livermore, and Q. Mu, "Preventing DC over-voltage in multi-terminal HVDC transmission," *CSEE J. Power Energy Syst.*, vol. 1, no. 1, pp. 86–94, Mar. 2015.
[10] S. Nanou and S. Papathanassiou, "Evaluation of a communication-based fault ride-through scheme for offshore wind farms connected through high-voltage DC links based on voltage source converter," *IET Renew. Power Generat.*, vol. 9, no. 8, pp. 882–891, Nov. 2015.
[11] A. Egea-Àlvarez, M. Aragüés-Peñalba, E. Prieto-Araujo, and O. Gomis-Bellmunt, "Power reduction coordinated scheme for wind power plants connected with VSC-HVDC," *Renew. Energy*, vol. 107, pp. 1–13, Jul. 2017.
[12] G. Ramtharan, A. Arulampalam, J. B. Ekanayake, F. M. Hughes, and N. Jenkins, "Fault ride through of fully rated converter wind turbines with AC and DC transmission," *IET Renew. Power Gener.*, vol. 3, no. 4, pp. 426–438, Dec. 2009.
[13] D. Tzelepis, A. O. Rousis, A. Dyśko, C. Booth, and G. Strbac, "A new fault-ride-through strategy for MTDC networks incorporating wind farms and modular multi-level converters," *Int. J. Elect. Power Energy Syst.*, vol. 92, pp. 104–113, Nov. 2017.
[14] M. Ndreko, J. L. Rueda, M. Popov, and M. A. M. M. van der Meijden, "Optimal fault ride through compliance of offshore wind power plants with VSC-HVDC connection by meta-heuristic based tuning," *Electr. Power Syst. Res.*, vol. 145, pp. 99–111, Apr. 2017.
[15] L. Xu, L. Yao, and C. Sasse, "Grid integration of large DFIG-based wind farms using VSC transmission," *IEEE Trans. Power Syst.*, vol. 22, no. 3, pp. 976–984, Aug. 2007.
[16] C. Feltes, H. Wrede, F. W. Koch, and I. Erlich, "Enhanced fault ride-through method for wind farms connected to the grid through VSC-based HVDC transmission," *IEEE Trans. Power Syst.*, vol. 24, no. 3, pp. 1537–1546, Aug. 2009.
[17] S. I. Nanou and S. A. Papathanassiou, "Grid code compatibility of VSC-HVDC connected offshore wind turbines employing power synchronization control," *IEEE Trans. Power Syst.*, vol. 31, no. 6, pp. 5042–5050, Nov. 2016.
[18] R. Sharma, Q. Wu, S. T. Cha, K. H. Jensen, T. W. Rasmussen, and J. Østegaard, "Power hardware in the loop validation of fault ride through of VSC HVDC connected offshore wind power plants," *J. Mod. Power Syst. Clean Energy*, vol. 2, no. 1, pp. 23–29, Mar. 2014.
[19] S. I. Nanou, G. N. Patsakis, and S. A. Papathanassiou, "Assessment of communication-independent grid code compatibility solutions for VSC–HVDC connected offshore wind farms," *Electr. Power Syst. Res.*, vol. 121, pp. 38–51, Apr. 2015.
[20] M. Ndreko, M. Popov, and M. A. M. M. van der Meijden, "Study on FRT compliance of VSC-HVDC connected offshore wind plants during AC faults including requirements for the negative sequence current control," *Int. J. Elect. Power Energy Syst.*, vol. 85, pp. 97–116, Feb. 2017.
[21] T. K. Vrana, Y. Yang, D. Jovcic, S. Dennetière, J. Jardini, and H. Saad, "The CIGRE B4 DC grid test system," *CIGRE Electra Mag.*, vol. 270, pp. 10–19, Oct. 2013.
[22] J. Lee, E. Muljadi, P. Srensen, and Y. C. Kang, "Releasable kinetic energy-based inertial control of a DFIG wind power plant," *IEEE Trans. Sustain. Energy*, vol. 7, no. 1, pp. 279–288, Jan. 2016.
[23] K. Rouzbehi, S. S. H. Yazdi, and N. S. Shariati, "Power flow control in multi-terminal HVDC grids using a serial-parallel DC power flow controller," *IEEE Access*, vol. 6, pp. 56934–56944, 2018.
[24] Z. Li, Y. Li, R. Zhan, Y. He, and X.-P. Zhang, "AC grids characteristics oriented multi-point voltage coordinated control strategy for VSC-MTDC," *IEEE Access*, vol. 7, pp. 7728–7736, 2019.
[25] A. Raza, Y. Liu, K. Rouzbehi, M. Jamil, S. O. Gilani, X. Dianguo, and B. W. Williams, "Power dispatch and voltage control in multiterminal HVDC systems: A flexible approach," *IEEE Access*, vol. 5, pp. 24608–24616, 2017.
[26] A. A. van der Meer, M. Ndreko, M. Gibescu, and M. A. M. M. van der Meijden, "The effect of FRT behavior of VSC-HVDC-connected offshore wind power plants on AC/DC system dynamics," *IEEE Trans. Power Del.*, vol. 31, no. 2, pp. 878–887, Apr. 2016.
[27] M. Abdollahi, J. I. Candela, J. Rocabert, R. S. M. Aguilar, and P. Rodriguez, "Active power limiter for grid connection of modern renewable SSG SPC," in *Proc. 6th Int. Conf. Renew. Energy Res. Appl. (ICRERA)*, Nov. 2017, pp. 728–733.
[28] S. S. H. Yazdi, J. Milimonfared, S. H. Fathi, K. Rouzbehi, and E. Rakhshani, "Analytical modeling and inertia estimation of VSG-controlled type 4 WTGs: Power system frequency response investigation," *Int. J. Elect. Power Energy Syst.*, vol. 107, pp. 446–461, May 2019.
[29] S. S. H. Yazdi, J. Milimonfared, and K. Rouzbehi, "Incorporation of synchronous power controlled energy storage system in wind farms to provide inertial and primary frequency support," in *Proc. Iran. Conf. Elect. Eng. (ICEE)*, May 2018, pp. 1379–1384.
[30] S. S. H. Yazdi, J. Milimonfared, and K. Rouzbehi, "Inertial support by a synchronous power controlled type 4 wind turbine: A restructured control approach," in *Proc. Iran. Conf. Elect. Eng. (ICEE)*, May 2018, pp. 1373–1378.
[31] A. D. Paquette, M. J. Reno, R. G. Harley, and D. M. Divan, "Sharing transient loads : Causes of unequal transient load sharing in islanded microgrid operation," *IEEE Ind. Appl. Mag.*, vol. 20, no. 2, pp. 23–34, Apr./Mar. 2014.
[32] D. Tzelepis, S. M. Blair, A. Dyśko, and C. Booth, "DC busbar protection for HVDC substations incorporating power restoration control based on dyadic sub-band tree structures," *IEEE Access*, vol. 7, pp. 11464–11473, 2019.
[33] A. Raza, A. Akhtar, M. Jamil, G. Abbas, S. O. Gilani, L. Yuchao, M. N. Khan, T. Izhar, X. Dianguo, and B. W. Williams, "A protection scheme for multi-terminal VSC-HVDC transmission systems," *IEEE Access*, vol. 6, pp. 3159–3166, 2017.